Supplementary figures 1 to 4 of:

Synchro-PASEF allows precursor-specific fragment ion extraction and interference removal in data-independent acquisition

Patricia Skowronek, Florian Krohs, Markus Lubeck, Georg Wallmann, Ericka C.M. Itang, Polina Koval, Maria Wahle, Marvin Thielert, Florian Meier, Sander Willems, Oliver Raether, Matthias Mann

	Standard method	Method 2 (Fig. 3)
MS1 scan	100 ms	100 ms
synchro scans	4 x 100 ms	7 x 100 ms
transfer time	5 x 12.3 ms	8 x 12.3 ms
total cycle time	561 ms = 0.56 s	899 ms

Supplementary Table 1: Cycle time parameters.

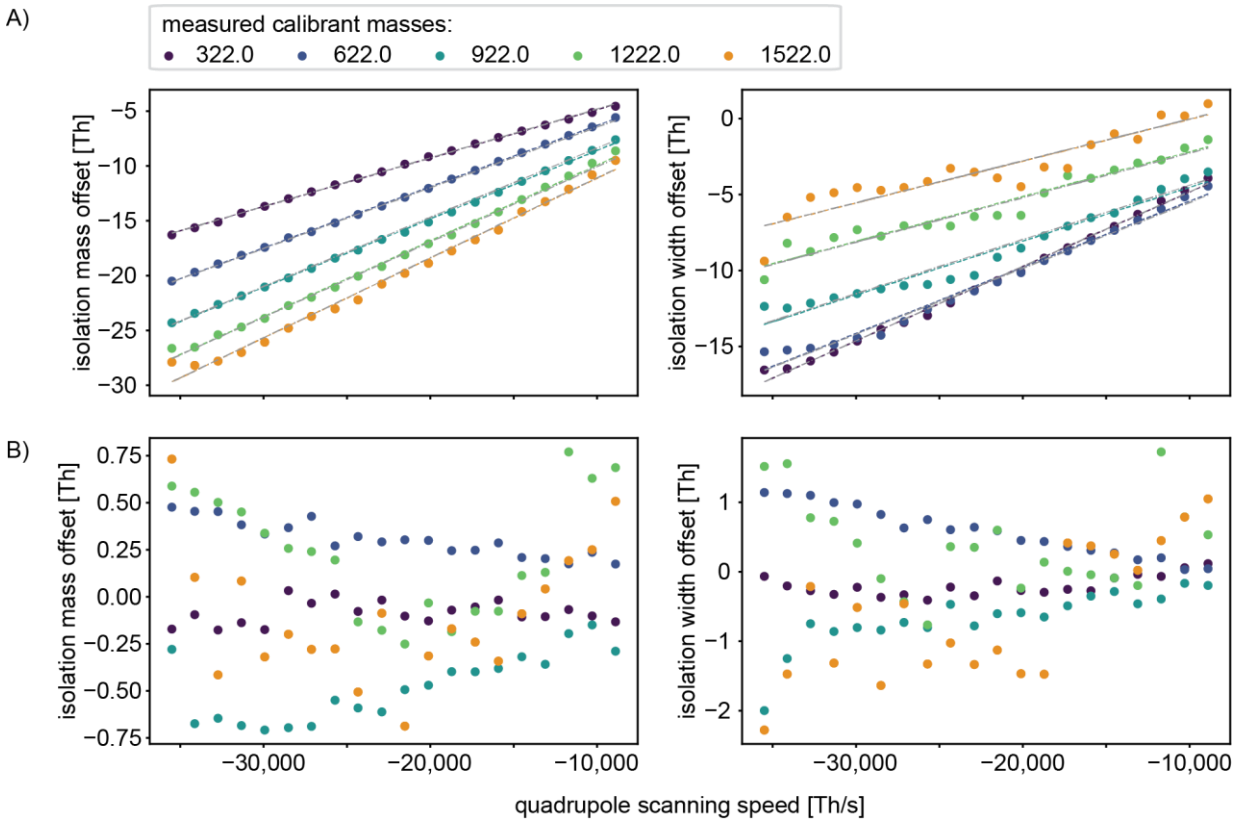

Supplementary Figure S1: Precision of the quadrupole depending on quadrupole scanning speed.

For this experiment a constant quadrupole isolation width of 25 Th was used.

A) Before quadrupole calibration. The position of the isolation window shows linear behavior with the quadrupole scanning speed (left panel). The width of the isolation window behaves less linear than the position when varying the quadrupole scanning speed (right panel)

B) After quadrupole calibration. The resulting isolation mass position offset is within ± 0.75 Th (left) and the resulting offset of the isolation window width is about ± 2 Th.

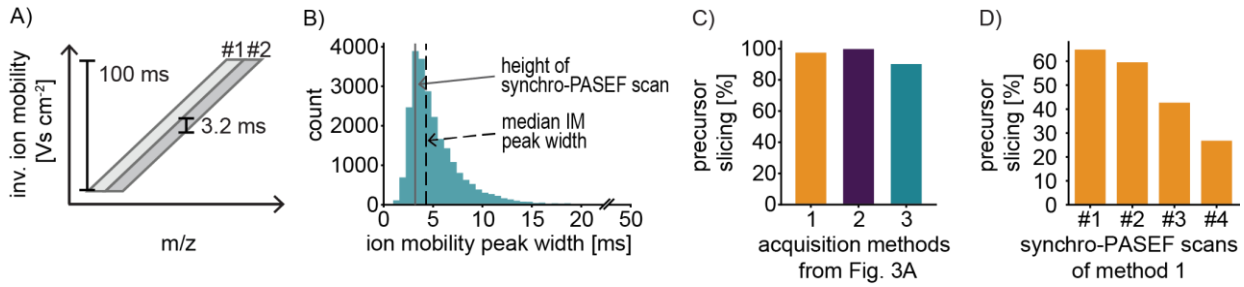

Supplementary Figure S2: Precursor slicing is a nearly universal phenomenon.

A) The TIMS tunnel releases precursor ions according to their ion mobility for 100 ms. The diagonal scan line has an isolation width of 25 Th and a height of 0.019 Vs cm^{-2}, corresponding to 3.2 ms.

B) Histogram of ion mobility peak widths from the HeLa reference library (see Experimental Procedures). The median is at 0.026 Vs cm^{-2}, corresponding to 4.3 ms. 21% of the peaks have an ion mobility width smaller than the height of the diagonal scan line.

C) Percentage of precursor slicing calculated with the dda-PASEF, HeLa run from Figure 3A. Note that only precursors with (part of their) ion mobility within the scan area are considered.

D) Percentage of precursor slicing per synchro scan for method 1.

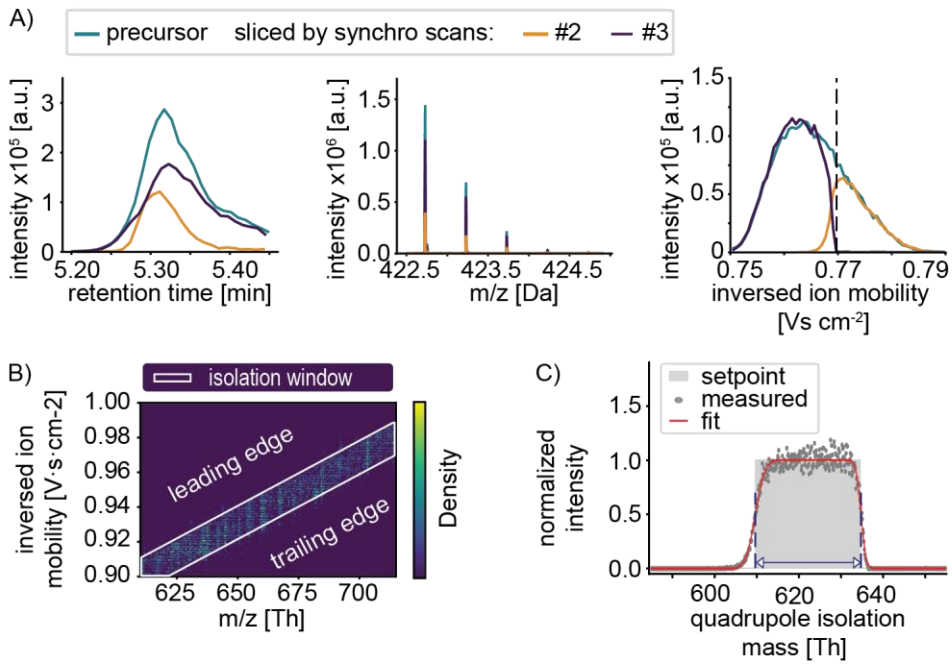

Supplementary Figure S3: Precursor slicing in the ion mobility dimension

A) The plots show the peptide SIPETQK of the simple protein mixture acquired with minimal collision energy. The precursor signal and the signals, that are sliced by the synchro scans, align in the retention time dimension (left panel). The isotopic peak patterns of the adjacent synchro scans follow the expected intensity pattern (middle panel). The ion mobility dimension shows precursor slicing and confirms that both sliced peak parts conform to the precursor peak shape (right panel).

B) The left panel shows the isolated signal of a single synchro scan. In the right panel, the isolated signal is overlayed with the programmed isolation window in grey. The heatmaps demonstrate that the leading edge is exact and the trailing edge is somewhat softer.

C) The programmed quadrupole shape is rectangular (colored in light grey) and the actual quadrupole shape in red is fitted based on measured data points.

Description for: 'Pure fragmentation spectra' in complex mixtures

For a preliminary but unbiased evaluation of the discriminatory power of precursor slicing, we analyzed the simple protein mixture spiked into a complex cellular lysate background (see main text). A data set was generated consisting of the 268 peptides identified by a MaxQuant search (1) from which the precursor position and dimensions were retrieved. Fragment intensities were predicted in silico using AlphaPeptDeep (2) for comparison in mirrored spectra (**Fig. 5G**).
We set out to generate pure fragmentation spectra for the 40 peptides around the dataset's median intensity value for the 268 peptides. While all precursors were sliced, only the 29 of them that had at least two recognized parts were considered for our analysis.
The peptide fragment extraction window was positioned based on the peptide's retention time, ion mobility, and m/z ratio allowing for a maximum tolerance to the library of 10 s, 0.03 IM and 20 ppm. The profile of the precursor species in the retention time and mobility dimension was determined by all scans where the intensity decreased monotonically symmetrically from the local intensity maximum. There were at least 11 datapoints in the RT and IM dimension and a maximum of 31 datapoints in the RT or IM dimension. We simulated slicing on the first two precursor isotopes (C12 and C13) by transforming the precursor peak with the quadrupole calibration function into partitions. This template was compared to all existing fragments with a total intensity over an estimated technical noise level of 500 units. This technical filter was applied for all calculations, both the unprocessed and the pure fragmentation spectra.
The template for the expected fragment slicing in the two-dimensional retention time–ion mobility plane was correlated with all fragment mass slices. For every such potential fragment, the correlation of each peak part and the corresponding template was calculated. The mean correlation between the peak parts was used as a first quality metric. Furthermore, the summed intensity ratio between the two sliced parts was calculated. The absolute log2 deviation between the observed ratio and the template ratio was used as the second quality metric.
All potential fragments with a mean correlation above 0.2 and a deviation from the intensity ratio of less than 3 were accepted for the pure fragmentation spectra. Fragments were then annotated with a 20 ppm mass tolerance, and the annotated specificity, termed purity, was calculated as the filtered, annotated intensity divided by the total filtered intensity.

REFERENCES

1. Prianichnikov, N., Koch, H., Koch, S., Lubeck, M., Heilig, R., Brehmer, S., Fischer, R., and Cox, J. (2020) Maxquant software for ion mobility enhanced shotgun proteomics. *Mol. Cell. Proteomics* 19, 1058–1069
2. Zeng, W.-F., Zhou, X.-X., Willems, S., Ammar, C., Wahle, M., Bludau, I., Voytik, E., Strauss, M. T., and Mann, M. (2022) AlphaPeptDeep: A modular deep learning framework to predict peptide properties for proteomics. *bioRxiv*, 2022.07.14.499992

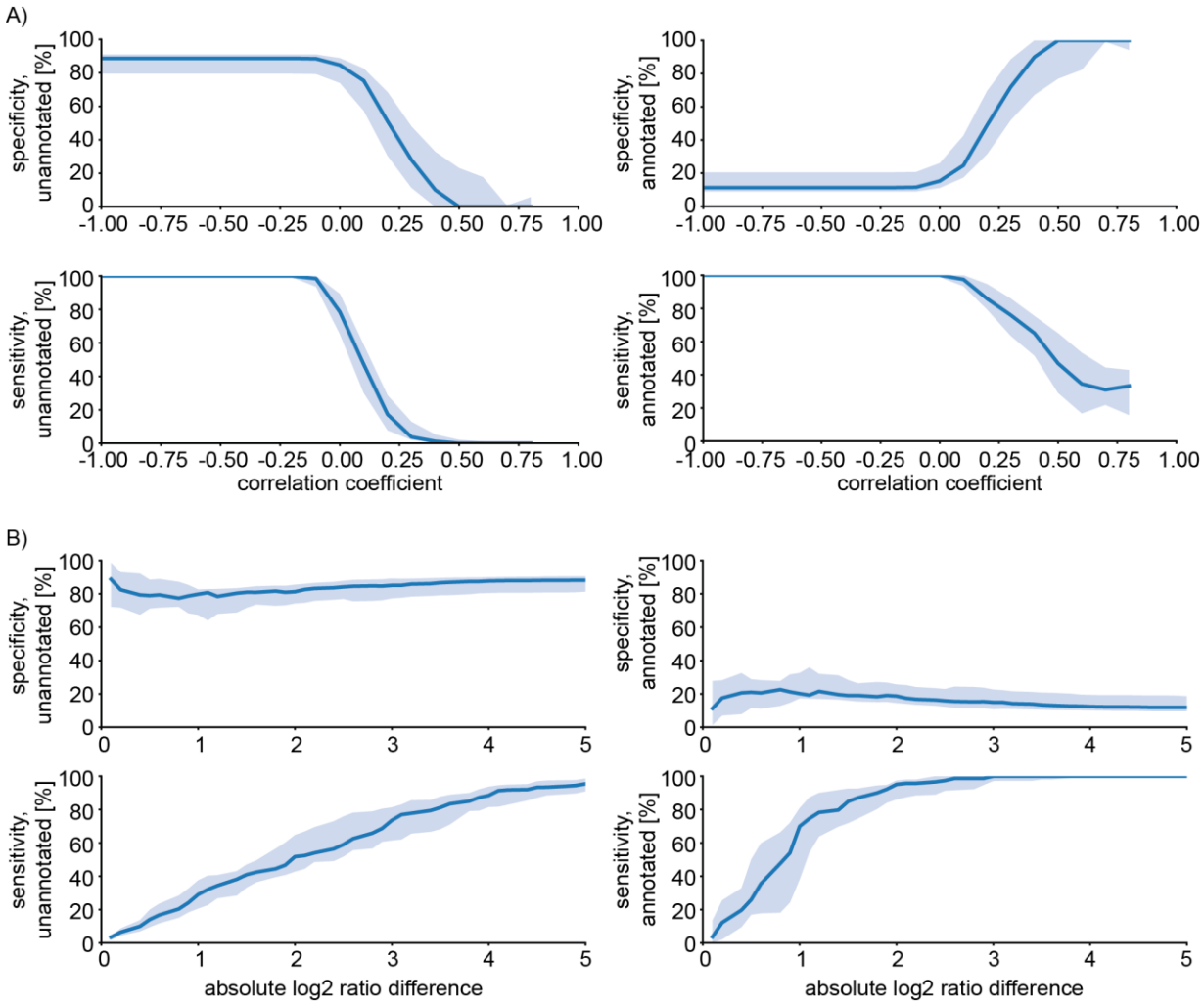

Supplementary Figure S4: Systematic evaluation of filtering criteria for finding the right balance between pure fragmentation spectra without losing annotated peaks.

A) Unannotated and annotated specificity and sensitivity as a function of the correlation coefficient. The median specificity is illustrated as blue line and the 75% interquartile range as light blue area. This calculation was performed on the 29 selected peptides as shown in supplementary Figure S5. The annotated specificity is the filtered, annotated intensity divided by the total filtered intensity. The unannotated specificity is likewise calculated as the sum of the unannotated intensity divided by the total filtered intensity. The purity score is equivalent to the specificity for annotated peaks. The annotated sensitivity is the filtered, annotated intensity divided by the unfiltered, annotated intensity. The unannotated sensitivity is the filtered, unannotated intensity divided by the unfiltered, unannotated intensity. Filtered and unfiltered refers to the quality filters, correlation and ratio deviation.

In all cases, noise was removed for this evaluation by requiring a minimum total intensity of 500.

B) Unannotated and annotated specificity and sensitivity as a function of the absolute log2 ratio difference.

Supplementary Figure S5: Complex and pure fragmentation spectra.

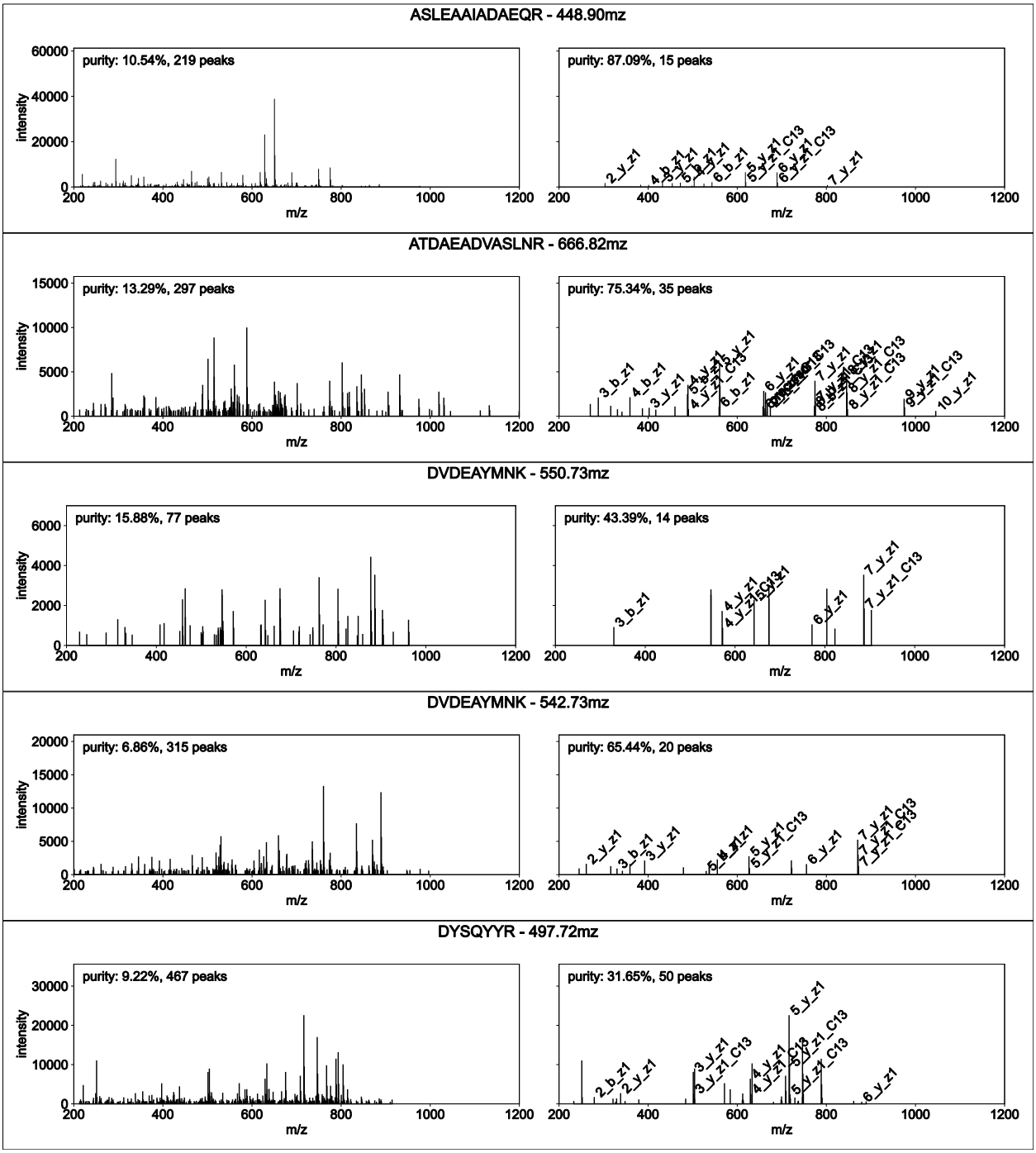

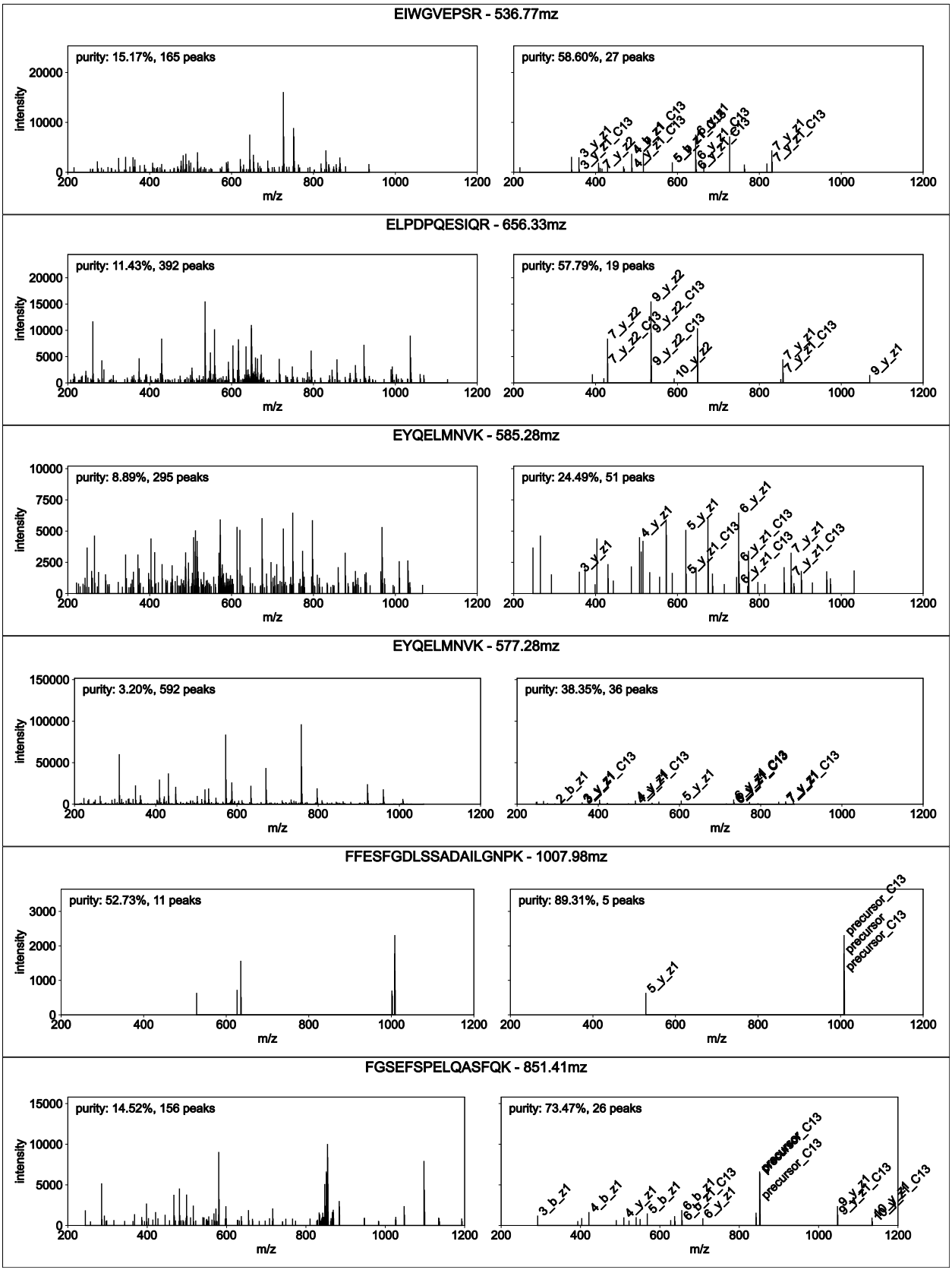
EIWGVEPSR - 536.77mz
purity: 15.17%, 165 peaks
purity: 58.60%, 27 peaks
ELPDPQESIQR - 656.33mz
purity: 11.43%, 392 peaks
purity: 57.79%, 19 peaks
EYQELMNVK - 585.28mz
purity: 8.89%, 295 peaks
purity: 24.49%, 51 peaks
EYQELMNVK - 577.28mz
purity: 3.20%, 592 peaks
purity: 38.35%, 36 peaks
FFESFGDLSSADAILGNPK - 1007.98mz
purity: 52.73%, 11 peaks
purity: 89.31%, 5 peaks
FGSEFSPELQASFQK - 851.41mz
purity: 14.52%, 156 peaks
purity: 73.47%, 26 peaks
intensity
m/z

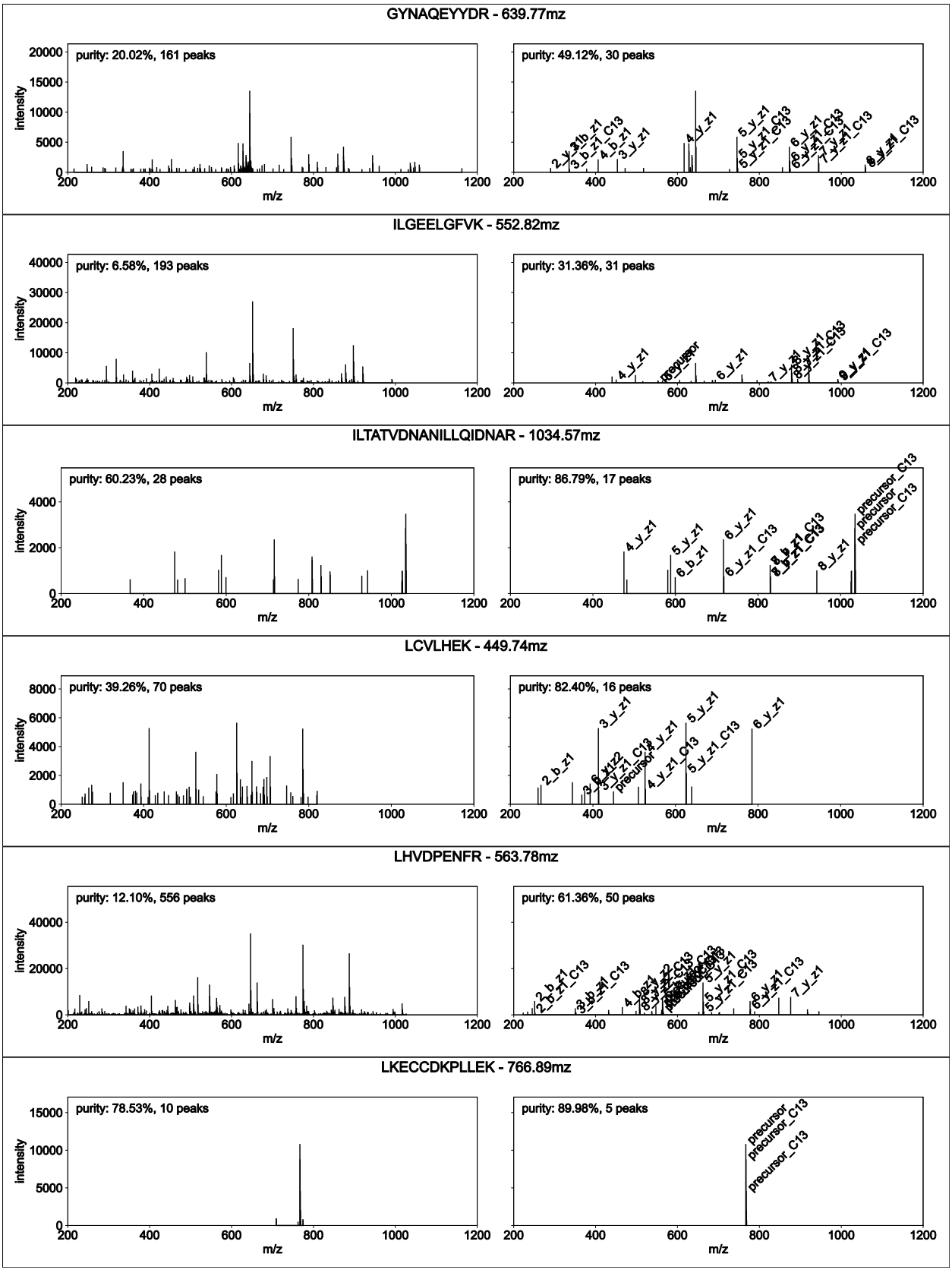
GYNAQEYYDR - 639.77mz
purity: 20.02%, 161 peaks
purity: 49.12%, 30 peaks
ILGEELGFVK - 552.82mz
purity: 6.58%, 193 peaks
purity: 31.36%, 31 peaks
ILTATVDNANILLQIDNAR - 1034.57mz
purity: 60.23%, 28 peaks
purity: 86.79%, 17 peaks
LCVLHEK - 449.74mz
purity: 39.26%, 70 peaks
purity: 82.40%, 16 peaks
LHVDPENFR - 563.78mz
purity: 12.10%, 556 peaks
purity: 61.36%, 50 peaks
LKECCDKPLLEK - 766.89mz
purity: 78.53%, 10 peaks
purity: 89.98%, 5 peaks
intensity
m/z

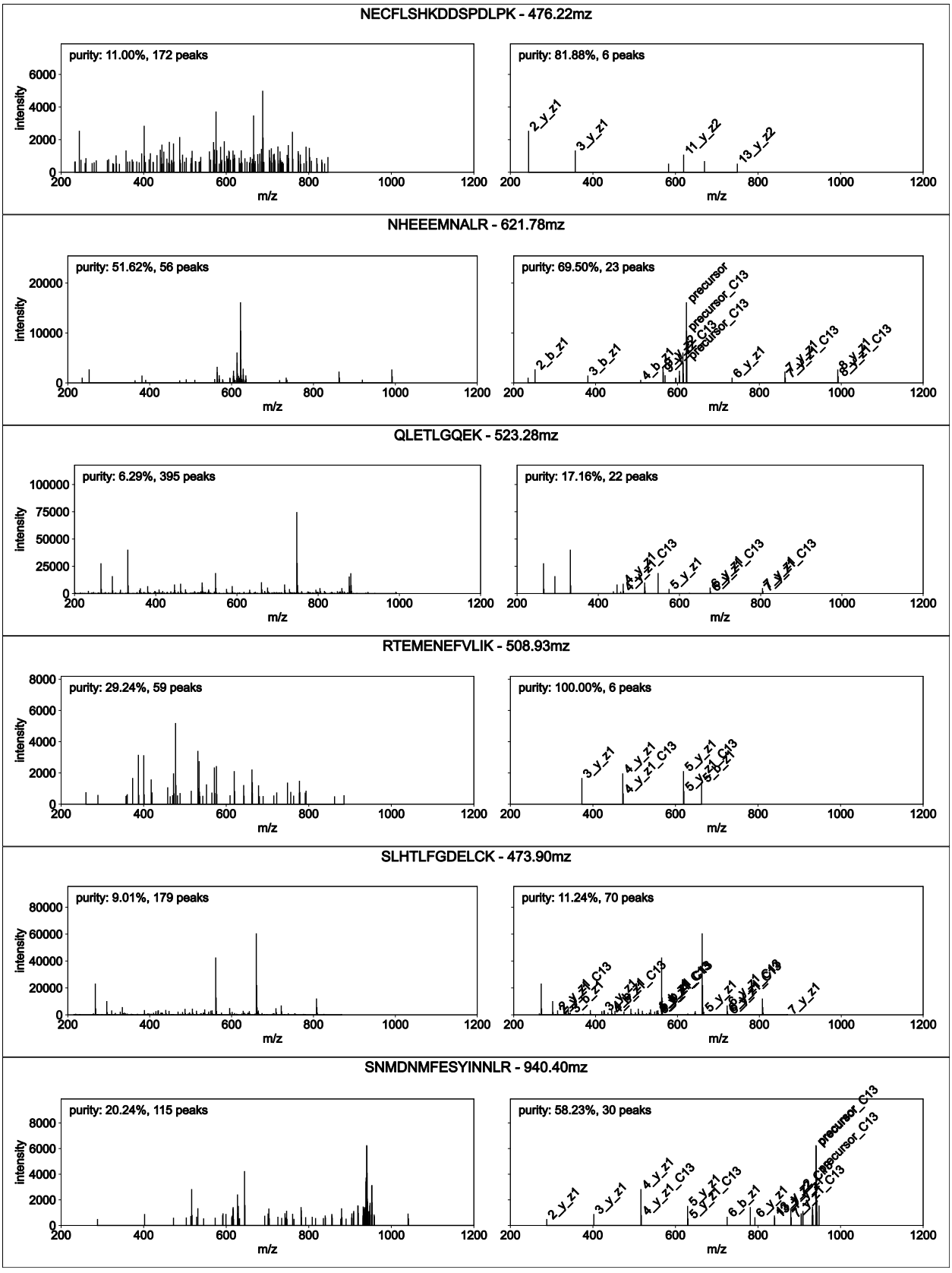
NECFLSHKDDSPDLPK - 476.22mz
purity: 11.00%, 172 peaks
purity: 81.88%, 6 peaks
2_y_z1
3_y_z1
11_y_z2
13_y_z2
NHEEEMNALR - 621.78mz
purity: 51.62%, 56 peaks
purity: 69.50%, 23 peaks
precursor
precursor_C13
2_b_z1
3_b_z1
6_y_z1
QLETLGQEK - 523.28mz
purity: 6.29%, 395 peaks
purity: 17.16%, 22 peaks
5_y_z1
RTEMENEFVLIK - 508.93mz
purity: 29.24%, 59 peaks
purity: 100.00%, 6 peaks
3_y_z1
4_y_z1
4_y_z1_C13
5_y_z1
SLHTLFGDELCK - 473.90mz
purity: 9.01%, 179 peaks
purity: 11.24%, 70 peaks
7_y_z1
SNMDNMFESYINNLR - 940.40mz
purity: 20.24%, 115 peaks
purity: 58.23%, 30 peaks
2_y_z1
6_b_z1
intensity
m/z

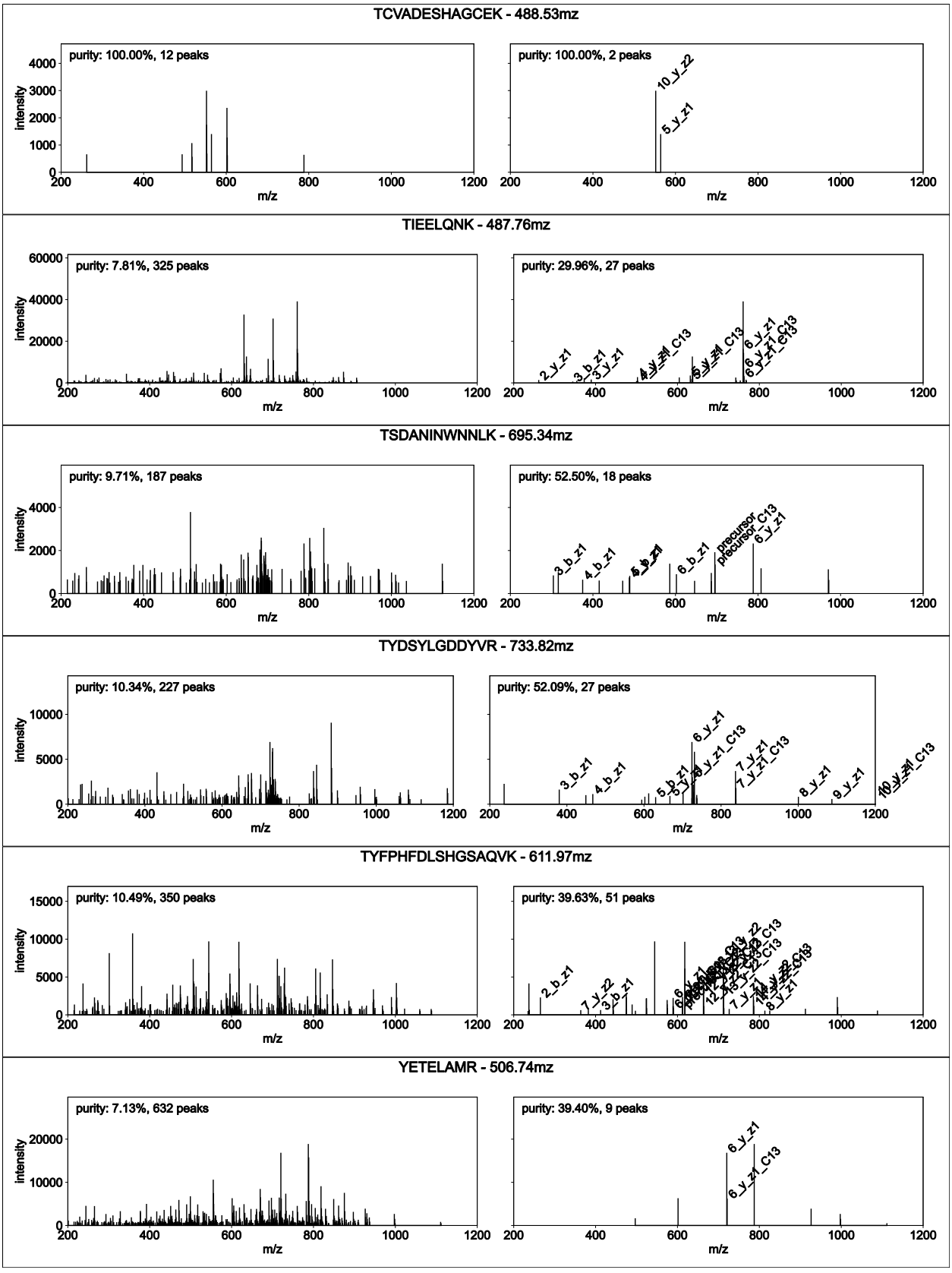
TCVADESHAGCEK - 488.53mz
purity: 100.00%, 12 peaks
purity: 100.00%, 2 peaks
10_y_z2
5_y_z1
TIEELQNK - 487.76mz
purity: 7.81%, 325 peaks
purity: 29.96%, 27 peaks
2_y_z1
3_b_z1
3_y_z1
4_y_z1_C13
5_y_z1_C13
6_y_z1
6_y_z1_C13
TSDANINWNNLK - 695.34mz
purity: 9.71%, 187 peaks
purity: 52.50%, 18 peaks
3_b_z1
4_b_z1
6_b_z1
precursor
precursor_C13
6_y_z1
TYDSYLGDDYVR - 733.82mz
purity: 10.34%, 227 peaks
purity: 52.09%, 27 peaks
3_b_z1
4_b_z1
5_b_z1
6_y_z1
6_y_z1_C13
7_y_z1
7_y_z1_C13
8_y_z1
9_y_z1
10_y_z1_C13
TYFPHFDLSHGSAQVK - 611.97mz
purity: 10.49%, 350 peaks
purity: 39.63%, 51 peaks
2_b_z1
7_y_z2
3_b_z1
8_y_z1
YETELAMR - 506.74mz
purity: 7.13%, 632 peaks
purity: 39.40%, 9 peaks
6_y_z1
6_y_z1_C13
intensity
m/z

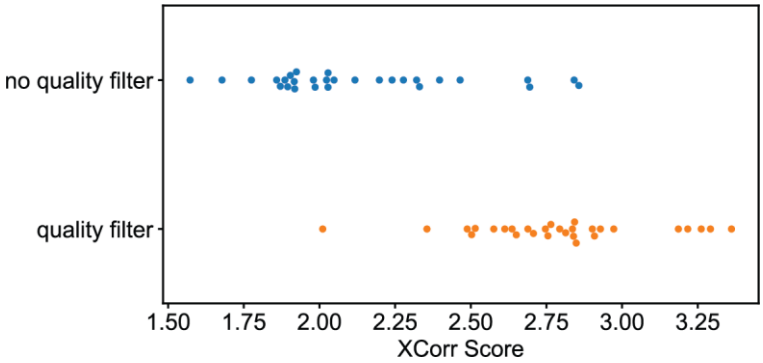

Supplementary Figure S6: Xcorr score for assessing the impact of precursor slicing on the spectra quality.

For the cross correlation score a fragment template was created using fragment masses calculated by AlphaPeptDeep. The template assigns a value of 1 to all datapoints within a 20ppm range of the first monoisotopic peak, a value of 0.5 to all datapoints of the second monoisotopic peak and a value of 0.25 to the third monoisotopic peak. The template as well as the unfiltered and filtered spectra were represented as dense signal with 394542 datapoints extending from 100.0 1700.0 Th, as defined by the timsTOF platform. The XCorr score was calculated as the log10 dot product of the template and the spectrum subtracted by the log10 mean cross correlation between the template and the spectrum for all possible offsets in the interval [-800, 0) and (0, 800].

peptide	precursor-fragment associations	interference
ASLEAAIADAEQR	x	
ATDAEADVASLNR		
DVDEAYoxMNK	x	
DVDEAYMNK	x	
DYSQYYR	x	
EIWGVEPSR	x	
ELPDPQESIQR	x	
EYQELoxMNVK	x	x
EYQELMNVK	x	x
FFESFGDLSSADAILGNPK		
FGSEFSPELQASFQK	x	x
GYNAQEYYDR	x	
ILGEELGFVK	x	
ILTATVDNANILLQIDNAR		
LCVLHEK		x
LHVDPENFR	x	x
LKECCDKPLLEK	x	
NECFLSHKDDSPDLPK	x	
NHEEEMNALR		
QLETLGQEK	x	
RTEoxMENEFVLIK	x	
SLHTLFGDELCK	x	
SNoxMDNoxMFESYINNLR	x	
TCVADESHAGCEK		
TIEELQNK	x	x
TSDANINWNNLK		x
TYDSYLGDDYVR	x	
TYFPHFDLSHGSAQVK	x	
YETELAMR		x

Supplementary Table 2: Reasons for possible misassignment.